Excitation and Control of Plasma Wakefields by Multiple Laser Pulses: Supplementary Material

J. Cowley[1], C. Thornton[1], C. Arran[1], R. J. Shalloo[1], L. Corner[1], G. Cheung[1], C.D. Gregory[2], S.P.D. Mangles[3], N. H. Matlis[4], D. R. Symes[2], R. Walczak[1], and S. M. Hooker[1]

[1]John Adams Institute for Accelerator Science, University of Oxford, Denys Wilkinson Building, Keble Road, Oxford OX1 3RH, United Kingdom
[2]Central Laser Facility, Rutherford Appleton Laboratory, Didcot OX11 0QX, United Kingdom
[3]John Adams Institute for Accelerator Science, Blackett Laboratory, Imperial College London, London SW7 2AZ, United Kingdom
[4]Deutsches Elektronen-Synchrotron (DESY), Notkestraße 85, Hamburg 22607, Germany

1 Generation of pulse trains

Single, temporally-chirped pulses from the laser system were converted into trains of pulses by placing a Michelson interferometer between the final laser amplifier and its vacuum compressor[1]. The Michelson comprised a 12.5 mm thick BK7 glass beam splitter which split the uncompressed laser beam and directed it into two arms terminated by four-inch diameter dielectric mirrors. One of these mirrors was mounted on a translation stage, which allowed the path difference, Δx, between the two Michelson arms to be adjusted. The angles of the beam splitter and the Michelson mirrors were chosen so that the beam reflected from the Michelson returned at a small angle to the incident beam, and so did not damage the laser amplifiers. The other output beam was sent via three four-inch diameter dielectric mirrors to the vacuum compressor.

The pulse train Michelson and compressor combination could be operated in two ways. If the compressor was set to compress fully the output of *each* arm of the Michelson, then with both arms of the Michelson open the output of the compressor comprised a pair of short (approximately 50 fs) pulses temporally separated by $\delta\tau = \Delta x/c$.

If the compressor was adjusted to give partial compression of the pulses in each arm of the Michelson, then its output comprised two chirped pulses separated in time by $\Delta x/c$; this created a pulse train, as follows. Suppose that a single chirped pulse from the compressor can be written in the form $E_{\mathrm{dr}}(t) = f_{\mathrm{dr}}(t - z/c)\cos\left[kz - \omega_0 t + \phi_{\mathrm{dr}}(t)\right]$, where $f_{\mathrm{dr}}(t - z/c)$ is the pulse envelope, and $\phi_{\mathrm{dr}}(t)$ is temporal phase of the drive pulse. The sum of two such pulses separated by $\Delta x/c$ — provided that the change in the pulse envelope in a time $\Delta x/c$ is small — comprises the envelope and carrier wave of either individual pulse modulated by the term,

$$f_{\mathrm{dr,mod}}(t) = \cos\left[\frac{\phi_{\mathrm{dr}}(t + \Delta x/c) - \phi_{\mathrm{dr}}(t) - \omega_0 \Delta x/c}{2}\right].$$

The combined pulses therefore form a pulse train with a temporal intensity profile equal to that of one of the chirped pulses modulated by a cosine-squared function. The pulses in the train occur when the argument of $f_{\mathrm{dr,mod}}(t)$ is a multiple of π. By expanding the temporal phase $\phi_{\mathrm{dr}}(t)$ in a Taylor series of the form $\phi_{\mathrm{dr}}(t) = \sum_{n=0}^{\infty} \frac{1}{n!}\phi_{\mathrm{dr}}^{(n)}(t - t_0)^n$, it is easy to show that the pulse spacing is given by $\delta\tau = 2\pi c/\phi_{\mathrm{dr}}^{(2)}\Delta x$. Note that the same conclusion is reached by considering the pulse train Michelson to be a spectral filter of angular free-spectral range $\Delta\omega_{\mathrm{FSR}} = 2\pi c/\Delta x$: since the rate of change of

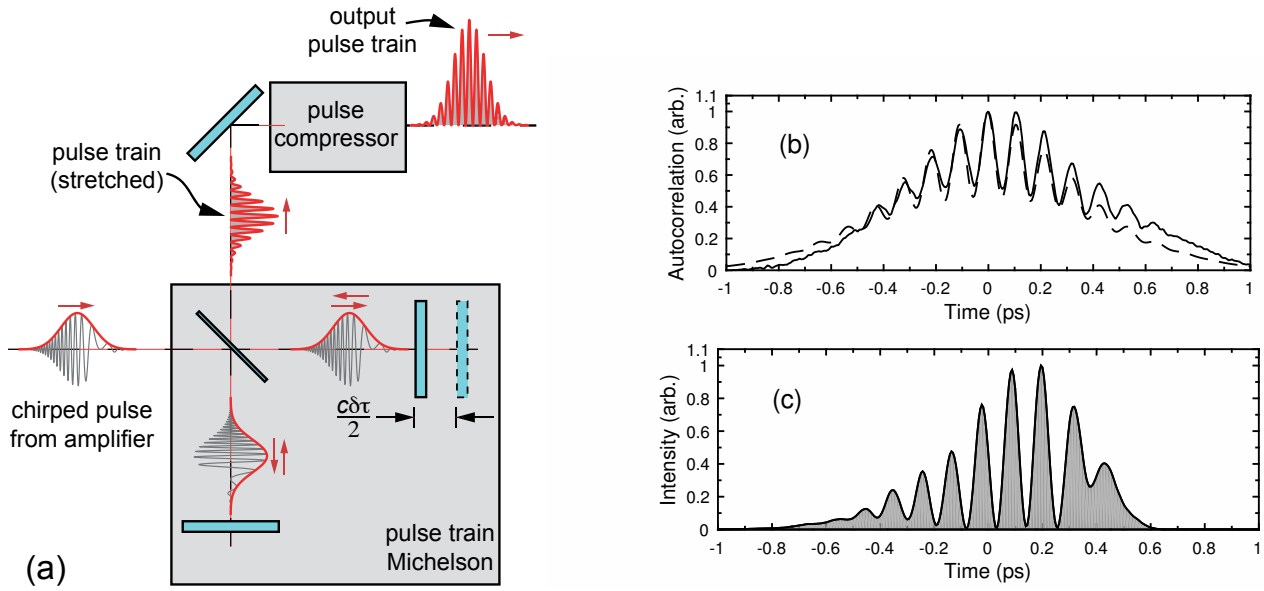

Figure 1: Generation of trains of pulses from a single pulse from the Gemini (Astra TA2) laser. (a) shows conceptually how the pulse trains were generated. Single, chirped pulses from the laser system were directed to a Michelson interferometer with a path difference between the two arms equal to $c\delta\tau$. The output of the Michelson therefore comprised two copies of the input chirped pulse, separated in time by $\delta\tau$; these pulses were directed to the laser vacuum compressor. If the compressor was set to give full compression then the output would comprise two, short pulses separated by $\delta\tau$. For other settings of the compressor the output would be a train of pulses, with total duration approximately equal to that of the pulse output by the compressor when one arm of the Michelson was blocked, and with a pulse separation determined by $\delta\tau$ and the separation of the gratings in the compressor. (b) shows an example of an autocorrelation measured with the SSA (solid line), together with the fit (dashed line) to the measured autocorrelation calculated from a model of the Michelson and vacuum compressor. (c) shows the temporal intensity profile of the pulse train deduced from the fit shown in (b).

frequency of the chirped pulses is given by $\omega_{\rm eff} = -{\rm d}\phi_{\rm dr}(t)/{\rm d}t = -\phi^{(2)}_{\rm dr}(t - t_0) + \ldots$, the temporal interval between frequencies transmitted by the Michelson and compressor combination is given by $\left|\phi^{(2)}_{\rm dr}\right| \delta\tau = \Delta\omega_{\rm FSR}$.

To generate the $N = 7$ pulse train shown in the main text, the grating spacing in the compressor was increased by approximately 1 mm, and hence the pulse train was negatively chirped, i.e. the instantaneous frequency decreased from the back to the front of the train.

To ensure a linear chirp, and thus a uniformly-spaced pulse train, an acousto-optic programmable dispersive filter was used to compensate for any third or fourth order phase arising from the laser system or the optics in the target area. Addition of the optimum amount of third- or higher-order phase was accomplished by monitoring the generated pulse trains with the single-shot autocorrelator described below.

The temporal intensity profile of the pulse train was determined by combining measurements of its spectrum and autocorrelation with a model of the pulse train Michelson and the compressor.[2] The spectrum of the pulse train was recorded by a spectrometer (Ocean Optics HR 4000) located between the pulse train Michelson and the compressor. A single-shot autocorrelator was used to record the autocorrelation of the pulse train; for these measurements a 25 mm diameter silver-coated mirror was introduced into the beam path which directed a portion of the pulse train beam through a 1 mm thick fused silica window in the vacuum chamber and to the SSA. Figure 1(b) shows an example of the measured autocorrelation. The recorded spectrum and autocorrelation could then be fitted to that

predicted by the model, allowing the grating separation, the other parameters of the compressor, and the path difference of the pulse train Michelson to vary within their experimental uncertainties. The effect of the thin window between the vacuum chamber and the SSA was also accounted for. This procedure allowed the temporal intensity profile of the pulse train to be deduced. Note, in contrast to an SSA measurement on its own, it was possible to determine the direction of time for the deduced pulse train since the sign of the GDD of the compressor was known.

The transverse intensity profiles of the focused pulse trains were measured by a CCD camera mounted in the vacuum chamber and calibrated with a USAF test chart.

2 Generation of probe and reference pulses

The probe and reference pulses were formed from an uncompressed 800 nm pulse transmitted by a partially reflecting mirror located after the second amplifier of the laser system. This pulse was compressed to a duration of approximately 50 fs in a dedicated compressor; passed through a soft aperture to yield a beam of 3.1 mm diameter and high spatial quality; and frequency doubled in a 600 μm thick beta barium borate (BBO) crystal. The probe and reference pulses were generated from this single 400 nm pulse by sending it to a Michelson interferometer containing a 1 inch diameter, 6.48 mm thick beam-splitter (IDEX PW1-1025UV); the path difference between the two arms was set to give $\Delta t \approx 5.5$ ps.

The probe and reference pulses leaving the Michelson were directed to an optical delay line which enabled their timing with respect to the drive laser pulse(s) to be adjusted. The retro-reflector of this delay line was mounted on a stepper motor (Thorlabs DRV014) with a step size of 2 μm. After leaving the delay line, the diagnostic pulses were passed through a half-wave plate so that their polarization was orthogonal to that of the drive pulse(s); this enabled any blue radiation generated in the target by the pump pulses to be blocked by a linear polarizer located before the spectrometer. The diagnostic pulses were then temporally stretched to a duration of approximately 1.5 ps by passing them through a 160 mm long block of BK7 glass.

The temporal chirp of the diagnostic pulses was measured in a separate experiment: the diagnostic pulse to be characterized was focused along with a single, fully-compressed 50 fs drive pulse into the gas cell, which contained approximately 30 mbar of hydrogen. The spectrum of the diagnostic pulse was strongly modulated when the drive pulse coincided with part of its temporal profile; this modulation arose from the rapid ionization of the gas by the drive pulse, and was centred at the local wavelength $\lambda(t)$ of the chirped diagnostic pulse. Hence $\lambda(t)$ could be measured by tracking the centre of the modulation as the delay between the drive and probe/reference pulse was varied. These measurements yielded the frequency of the probe/reference pulse as a function of time, $\omega(t) = -\mathrm{d}\phi/\mathrm{d}t$, where $\phi(t)$ is the temporal phase of the probe/reference pulse. Expanding the temporal phase as $\phi(t) = \sum_{n=0}^{\infty} \frac{1}{n!}\phi^{(n)}(t-t_0)^n$, the parameter $\phi^{(2)}$ can be extracted from a polynomial fit to $\omega(t)$, which yields the group delay dispersion of the pulse, $\psi^{(2)}$, since for a strongly chirped pulse $\psi^{(2)} = -1/\phi^{(2)}$. The GDD was typically found to be $\psi^{(2)} \approx 24,500\,\mathrm{fs}^{-2}$, the precise value depending on the alignment through the glass block. The GDD of the reference pulse was found to be approximately $1500\,\mathrm{fs}^{-2}$ larger than that of the probe pulse since it passed through the beamsplitter of the diagnostic pulse Michelson three times, compared to a single transit for the probe pulse.

3 Design of gas cell

The target gas cell was machined from aluminium. Hydrogen gas was introduced to the cell via a pipe of 5 mm internal diameter. The laser pulses were coupled into and out of the cell through pinholes of 250 μm diameter drilled in 250 μm thick stainless steel and spaced by approximately 3 mm along the laser axis.

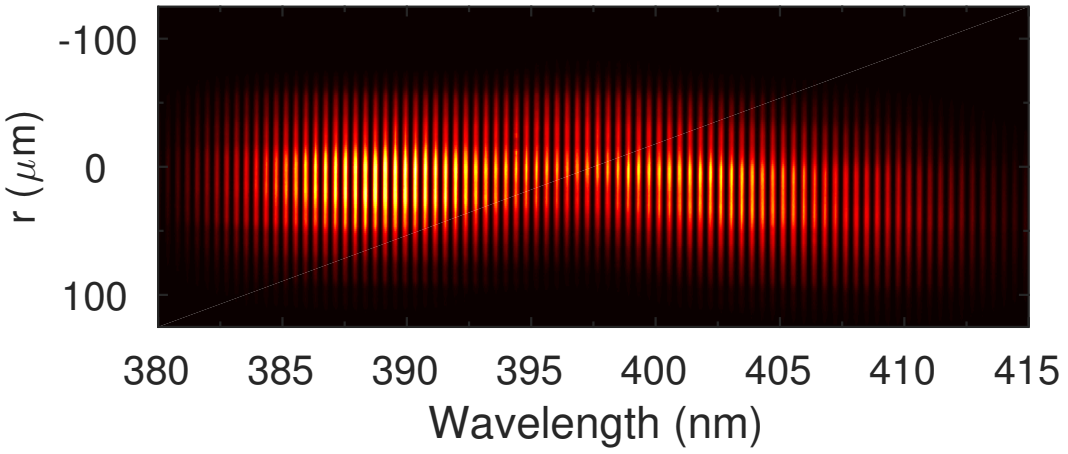

Figure 2: Example spectral interferogram.

4 Spectrometer set-up

After leaving the gas cell, the diagnostic pulses were separated from the drive pulse(s) by reflecting them from a dichroic mirror designed to reflect (transmit) 400 nm (800 nm) radiation. The diagnostic beam was then collimated by a $f = 1$ m, 75 mm diameter lens and passed out of the vacuum chamber through a 25 mm thick fused silica window. Once in air, the diagnostic beam was reduced in diameter by a factor of three by a Gallilean telescope, transmitted by an additional dichroic mirror which reflected any remaining 800 nm radiation, and transmitted through a prism polarizer oriented so as to block any blue radiation generated by the drive pulse(s). The diagnostic beam was then focused by a $f = 300$ mm, 25 mm diameter lens, and imaged onto the entrance slit of a grating spectrograph by a 10× planar apochromatic microscopic objective (Mitutoyo M plano APO Nuv10x) and tube lens. This optical system was set-up so as to image the rear pinhole of the gas cell onto the entrance slit of the spectrometer.

The spectrograph (Acton SpectraPro 2750) contained a 2400 grooves / mm grating which dispersed the spectra of the diagnostic pulses onto a CCD detector (Andor Newton, DU940N-BU) with 2048 by 512 pixels of dimensions 13.5 μm × 13.5 μm. The bandwidth captured by the spectrograph and CCD was approximately 13 nm. Calibration with an Air Force test target in the non-dispersed direction showed that each pixel of the CCD detector corresponded to 1.3 μm in the object plane.

5 Implementation of FDH and TESS analyses

Figure 2 shows a typical spectral interferogram obtained in the experiments. For each run background spectral interferograms were recorded with all laser pulses, but with the gas cell evacuated; these were used to isolate the spectral phase due to the wakefield from the intrinsic spectral phase of the probe and reference pulses. The measured probe GDD, $\psi^{(2)}$, was first used to calculate the probe's quadratic spectral phase $\frac{\psi^{(2)}}{2}(\omega - \omega_0)^2$, which was necessary to reconstruct the probe's electric field in the spectral domain. After a Fourier transform it was then used to calculate the corresponding quadratic temporal phase $-\frac{1}{2\psi^{(2)}}(t - t_0)^2$ which could then be subtracted from the electric field in the temporal domain to leave only the temporal phase due to the wakefield. During the Fourier transform of the probe's electric field the temporal resolution of the final FDH plots was improved to 2 fs by adding zero padding to the recorded spectrum to give an array sixteen times that of the spectrometer CCD.

The TESS analysis used the positive satellite to avoid the signal from the ionization front. The background — i.e. the DC peaks, the side-band, and extraneous peaks caused by weak back reflections — was subtracted by scaling and translating (in the spatial dimension) the background interferograms to match the sideband of the data shot. Satellite peaks were then identified automatically by searching

the region between 6 and 8.5 ps from the DC peak; only those peaks centred on regions of elevated signal extending at least 3 pixels spatially and 50 fs temporally were retained.

In order to calculate the satellite to sideband ratio, r_1, the background was further reduced by defining three grids of 8×8 pixels: one centred on the satellite; and two grids separated in the spatial dimension by 20 pixels (i.e. above and below the satellite). The average of the two grids above and below the satellite was then subtracted from the grid centred on the satellite, and the remaining signal was smoothed with a locally weighted linear regression fit.

The spectral overlap factors were calculated from eqn (2) in the main paper, using the background interferograms after applying a low pass frequency filter to remove the interference fringes.

The relative wake amplitude was calculated from eqn (1) in the main paper, using the measured satellite to sideband ratio, the measured probe central wavelength of 395 nm, the effective length of the gas, ℓ, and the plasma frequency calculated from the measured gas pressure. The effective length of gas was confirmed by measuring, as a function of cell pressure, the rate of change of the probe phase shift due to ionization of the target gas. The value deduced in this way, $\ell = 3$ mm, is consistent with the pinhole spacing.

Wakefields were observed in approximately 70% of shots. In order to reduce the error from shot to shot variation, the measured wake amplitudes were collated and averaged in 7-12 equally spaced pressure bins.

6 Calculation of wake amplitudes

In the linear regime the relative amplitude of the wakefield driven by laser radiation with a normalized vector potential a is given by,[3]

$$\frac{\delta n_\mathrm{e}}{n_{\mathrm{e}0}} = \frac{c^2}{2\omega_\mathrm{p}} \int_{-\infty}^{t} \mathrm{d}t' \sin\left[\omega_\mathrm{p}\left(t-t'\right)\right] \nabla^2 a^2. \tag{SM-1}$$

If we let $a^2 = a_0^2 f_\perp(r) f_\parallel(\zeta)$, where r is the radial distance from the axis of propagation, then far behind the driving laser pulse the amplitude of the plasma wave can be written as,

$$\frac{\delta n_\mathrm{e}}{n_{\mathrm{e}0}} = -\sqrt{\frac{\pi}{2}} \frac{c^2}{\omega_\mathrm{p}} a_0^2 \left[\frac{\omega_\mathrm{p}^2}{c^2} f_\perp(r) - \nabla_\perp^2 f_\perp(r)\right] \left|\tilde{f}_\parallel(\omega_\mathrm{p})\right|, \tag{SM-2}$$

where $\nabla_\perp^2$ is the transverse Laplacian operator, and $\tilde{f}_\parallel(\omega) = \sqrt{1/2\pi}\int_{-\infty}^{\infty} f_\parallel(\zeta) \exp\left(-\mathrm{i}\omega\zeta\right) \mathrm{d}\zeta$ is the Fourier transform of $f_\parallel(\zeta)$. Equation (SM-2) yields eqn (3) in the main text for the case of a single bi-Gaussian laser pulse with $f_\perp(r) = \exp\left[-2(r/w_0)^2\right]$ and $f_\parallel(\zeta) = \exp\left[-4\ln 2\,(\zeta/\tau)^2\right]$. To calculate the wake amplitude driven by the measured pulse trains, equation (SM-2) was solved numerically by assuming $f_\perp(r)$ as for the bi-Gaussian pulse; and replacing $f_\parallel(\zeta)$ with the measured temporal intensity profile, but with the temporal axis scaled by a factor α as explained in the main text.

7 Estimate of wakefield reduction by trailing, non-resonant pulse

The reduction in the wake amplitude is deduced from Fig 3(b) which shows the wake field measured as a function of the cell pressure. At pressures for which the separation of the two laser pulses was a multiple of the plasma period, the wake amplitude will be $A_\mathrm{res} = a_1 + a_2$, where a_1 and a_2 are the amplitudes of the wakefields driven by each laser pulse. For pressures at which the trailing laser pulse is out of resonance, the wakefield amplitude will be $A_\mathrm{non-res} = a_1 - a_2$. From Fig. 3(b) we find, for a pressure of $P \approx 10$ mbar, $A_\mathrm{res} = (0.87 \pm 0.12)\%$; for $P \approx 19$ mbar, $A_\mathrm{non-res} = (0.34 \pm 0.08)\%$. Solving these for $a_{1,2}$ we find $a_1 = (0.6 \pm 0.1)\%$ and $a_2 = (0.265 \pm 0.015)\%$. Hence a trailing, out-of-resonance

laser pulse decreases the amplitude of the wakefield from $a_1 = (0.6\pm0.1)\%$ to $A_{\mathrm{non-res}} \approx (0.34\pm0.08)\%$; this is a reduction of $(44 \pm 8)\%$.

References

1. Weling, A. S. & Auston, D. H. Novel sources and detectors for coherent tunable narrow-band terahertz radiation in free space. *J Opt Soc Am B* **13,** 2783–2791 (1996).
2. Shalloo, R. J. *et al.* Generation of laser pulse trains for tests of multi-pulse laser wakefield acceleration. *Nucl. Inst. Meth. A* **829,** 383–385 (2016).
3. Esarey, E., Schroeder, C. B. & Leemans, W. P. Physics of laser-driven plasma-based electron accelerators. *Rev. Mod. Phys.* **81,** 1229–1285 (2009).